Identifying network correlates of brain states using tensor decompositions of whole-brain dynamic functional connectivity

Nora Leonardi and Dimitri Van De Ville
Institute of Bioengineering, Ecole Polytechnique Fédérale de Lausanne (EPFL), Lausanne, Switzerland
Department of Radiology and Medical Informatics, University of Geneva, Geneva, Switzerland
{*nora.leonardi, dimitri.vandeville*}*@epfl.ch*

***Abstract*—Network organization is fundamental to the human brain and alterations of this organization by brain states and neurological diseases is an active field of research. Many studies investigate functional networks by considering temporal correlations between the fMRI signal of distinct brain regions over long periods of time. Here, we propose to use the higher-order singular value decomposition (HOSVD), a tensor decomposition, to extract whole-brain network signatures from group-level dynamic functional connectivity data. HOSVD is a data-driven multivariate method that fits the data to a 3-way model, i.e., connectivity $\times$ time $\times$ subjects. We apply the proposed method to fMRI data with alternating epochs of resting and watching of movie excerpts, where we captured dynamic functional connectivity by sliding window correlations. By regressing the connectivity maps' timecourses with the experimental paradigm, we find a characteristic connectivity pattern for the difference between the brain states. Using leave-one-subject-out cross-validation, we then show that the combination of connectivity patterns generalizes to unseen subjects as it predicts the paradigm. The proposed technique can be used as feature extraction for connectivity-based decoding and holds promise for the study of dynamic brain networks.**

***Keywords*-fMRI, dynamic functional connectivity, tensor decompositions**

I. Introduction

Functional magnetic resonance imaging (fMRI) is a powerful imaging tool for neuroscience to find neural correlates of cognition. Of particular interest today is the study of the brain as a network, whose architecture is subject to constant change during cognitive tasks [1], [2], [3] or even spontaneously [4], [5]. For example, Bassett *et al.* have shown extensive reorganization of network communities during motor learning [1]; and we have previously decoded brain states from functional connectivity graphs [2]. An emerging methodology is to look into whole-brain dynamic functional connectivity as extracted by correlation from a sliding temporal window [5]. As the number of connections increases quadratically with the number of brain regions, one remaining challenge is to robustly identify signatures of dynamic connectivity that relate to specific brain states, without reverting to summarizing measures such as clustering or modularity coefficients.

Exploratory and multivariate data analysis techniques like independent component analysis (ICA) and variations on principal component analysis (PCA) such as partial least squares [6] have been widely applied to fMRI activity timecourses to mine the "hidden" structure in brain organization. Next to bilinear decompositions (i.e., components have a spatial map and temporal loading), multisubject fMRI data can also be modelled using 3-way arrays or tensors (i.e., components have an additional subject loading as in tensor ICA [7]) or hierarchical models based on e.g. canonical correlation analysis [8]. Tensor decompositions, such as Tucker and Candecomp/Parafac, have become important tools in many fields as they explicitly exploit multiway structure in the data to disentangle multiple factors [9], [10]. In particular, the higher-order singular value decomposition (HOSVD) is a tensor generalization of SVD and corresponds to the Tucker decomposition with orthogonal factors, which guarantees uniqueness [11]. It is important to note that the 3-way structure—on the spatial, temporal, and subjects dimensions—exploits temporal consistency between subjects, which is the case for task-related data with identical experimental paradigms for all subjects, but not for resting state studies.

Here, we consider dynamic whole-brain functional connectivity estimated from fMRI data acquired during alternating epochs of resting and watching of movie excerpts. We then propose a 3-way model and decompose the data using HOSVD to retrieve connectivity maps with associated time courses and subject loadings. Within a leave-one-subject-out cross-validation scheme, we demonstrate that the technique can successfully identify connectivity maps that relate to the paradigm and generalize to the unseen subject. The proposed method can be used for feature extraction in future decoding schemes based on dynamic connectivity.

II. HOSVD of multisubject dynamic connectivity

Notations: Scalars are denoted by lowercase letters (e.g., a), vectors by boldface lowercase letters (e.g., $\mathbf{a}$), matrices by boldface capital letters (e.g., $\mathbf{A}$), and tensors by Euler script letters (e.g., $\mathcal{A}$). The dimensions of a tensor are also known as modes.

A. Data description

Paradigm: The experimental protocol consisted of 9 short movie excerpts (50 s) alternating with resting periods (90 s), for a total scanning duration of 23 minutes.

Data acquisition: We acquired data from $S = 15$ right-handed subjects without any history of neurological or psychiatric disorders, aged between 18 and 36

978-0-7695-5061-9/13 $26.00 © 2013 IEEE
DOI 10.1109/PRNI.2013.28

IEEE computer society

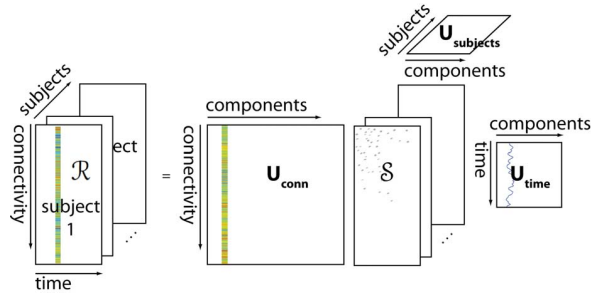

Figure 1: Multisubject dynamic connectivity is modeled using a third-order tensor *connections* $\times$ *time* $\times$ *subjects*. HOSVD decomposes a third order tensor $\mathcal{R}$ into a core tensor $\mathcal{S}$ and orthogonal mode matrices $\mathbf{U}_{\text{conn}}$, $\mathbf{U}_{\text{time}}$ and $\mathbf{U}_{\text{subjects}}$.

years [12]. fMRI data was acquired on a Siemens 3T TrioTIM (TR/TE/FA = 1.1s/27ms/90°, 21 axial slices, voxel size = 3.75×3.75×4.2mm^3, 1.05 mm gap). Structural data was acquired using a T1-weighted MPRAGE sequence (TR/TE/FA=1.9s/2.32 ms/9°, 192 axial slices, voxel size=0.90×0.90×0.90 mm^3).

Data preprocessing: All functional images were realigned using SPM8 and then parcellated into 90 regions according to the Automated Anatomical Labeling (AAL) atlas [13]. The use of an atlas helps to generalize the extracted connectivity maps across subjects. We excluded the bilateral pallidum due to signal dropout in some subjects, resulting in $N = 88$ brain regions, and averaged the activity of all voxels in each region.

Dynamic connectivity estimation: We estimated dynamic functional connectivity by calculating pair-wise windowed interregional correlations: $\rho_{xy}(t) = \text{corr}(x[t, t+\Delta t], y[t, t+\Delta t])$, where $t = 1, 11, ..., 1231$ and $\Delta t = 40$ is the window size, resulting in $T = 124$ windows for each subject. The step size and window length were chosen such as to limit computational demands and redundancy, while covering each movie excerpt (50s) with multiple windows. We then unfolded each subject's windowed correlation matrices and concatenated them across time to form a matrix of dynamic connectivity $\mathbf{R} = [\text{triu}(\mathbf{R}_1)|\text{triu}(\mathbf{R}_2)|...|\text{triu}(\mathbf{R}_T)] \in \mathbb{R}^{C\times T}$, with $C = (N^2-N)/2$. We retained only the upper triangular part due to symmetry.

B. 3-way model to identify group connectivity maps

We modelled multisubject dynamic connectivity by stacking the dynamic correlation matrices $\mathbf{R}$ of all subjects; i.e., we constructed a *connections* $\times$ *time* $\times$ *subjects* third-order tensor (see Fig. 1). We then used the HOSVD to orthogonalize the modes of the tensor $\mathcal{R} \in \mathbb{R}^{C\times T\times S}$ [11]:

$$\mathcal{R} = \mathcal{S} \times_1 \mathbf{U}_{\text{conn}} \times_2 \mathbf{U}_{\text{time}} \times_3 \mathbf{U}_{\text{subjects}} \tag{1}$$

where $\mathcal{S} \in \mathbb{R}^{C\times T\times S}$ is called the core tensor; $\mathbf{U}_{\text{conn}} \in \mathbb{R}^{C\times C}$, $\mathbf{U}_{\text{time}} \in \mathbb{R}^{T\times T}$, and $\mathbf{U}_{\text{subjects}} \in \mathbb{R}^{S\times S}$ are orthonormal mode matrices that span the connectivity, time and subject spaces, respectively (Fig. 1). $\mathcal{S} \times_n \mathbf{U}$ denotes the multiplication of a tensor $\mathcal{S} \in \mathbb{R}^{I_1\times I_2\times I_3}$ with a matrix $\mathbf{U} \in \mathbb{R}^{I_n\times I_n}$ in mode n. This corresponds to the multiplication $\mathbf{U}\mathbf{S}_{(n)}$ for the unfolded (matricized) tensor $\mathbf{S}_{(n)}$. $\mathbf{S}_{(n)}$ contains the columns, rows, or fibres of $\mathcal{S}$ for $n = 1, 2, 3$, respectively, as its columns: e.g., $\mathbf{S}_{(1)} \in \mathbb{R}^{I_1\times I_2 I_3}$ is a concatenation of the tensor's frontal slices (a frontal slice is a submatrix of the tensor obtained by fixing the third index and denoted as $\mathbf{S}_{::1}$).

The mode matrices $\mathbf{U}_{\text{conn}}, \mathbf{U}_{\text{time}}$ and $\mathbf{U}_{\text{subjects}}$ are computed from the SVD of the tensor $\mathcal{R}$ unfolded along each mode $n = 1, 2, 3$ [11]. For example, the columns in $\mathbf{U}_{\text{conn}}$ are the left singular vectors of $\mathbf{R}_{(\mathbf{1})}$: $\mathbf{R}_{(\mathbf{1})} = \mathbf{U}_{\text{conn}}\mathbf{D}\mathbf{V}^T$ with $\mathbf{R}_{(1)} \in \mathbb{R}^{C\times TS}$. As $\mathbf{R}_{(\mathbf{1})}$ contains temporally concatenated dynamic-connectivity data, $\mathbf{U}_{\text{conn}}$ is equivalent to "conventional" SVD. However, the core tensor $\mathcal{S}$ governs the interactions between the 3 modes and the columns of the transformed core tensor $\mathcal{S}^c = \mathcal{S} \times_1 \mathbf{U}_{\mathbf{conn}}$ are connectivity maps, which represent the principal axes of variation across time (mode 2) and subjects (mode 3).

Here, we are interested in the columns of $\mathbf{S^c}_{::1}$ because they are group connectivity maps. To see this, we first multiply Eq. (1) by $\mathbf{U}^T_{\text{subjects}}$ along mode 3, which gives

$$\mathcal{R} \times_3 \mathbf{U}^T_{\text{subjects}} = \mathcal{S}^c \times_2 \mathbf{U}_{\text{time}}, \tag{2}$$

since $(\mathcal{S}^c \times_2 \mathbf{U}_{\text{time}} \times_3 \mathbf{U}_{\text{subjects}}) \times_3 \mathbf{U}^T_{\text{subjects}} = \mathcal{S}^c \times_2 \mathbf{U}_{\text{time}} \times_3 (\mathbf{U}_{\text{subjects}}\mathbf{U}^T_{\text{subjects}})$ [11], [10]. We can interpret the frontal slices of $\mathcal{R}^s = \mathcal{R} \times_3 \mathbf{U}^T_{\text{subjects}}$ as weighted sums across all subjects' dynamic correlation matrices as we can write each frontal slice as $\mathbf{R^s}_{::k} = \sum_{s=1}^{S} u^{\text{subjects}}_{sk} \mathbf{R}_{::s}$ for $k = 1, ..., S$, where we used the notation from [14]. All entries in $\mathbf{u}^{\text{subjects}}_{:1}$ (the weights used to calculate $\mathbf{R^s}_{::1}$) have the same sign, which implies that the columns of the first frontal slice $\mathbf{R^s}_{::1}$ are weighted averages of dynamic connectivity across subjects.

Next, we show the correspondence between connectivity maps $\mathbf{S^c}_{::1}$ and the average dynamic connectivity $\mathbf{R^s}_{::1}$. We unfold $\mathcal{R}^s = \mathcal{S}^c \times_2 \mathbf{U}_{\text{time}}$ along mode 2 to obtain $\mathbf{R^s}_{(2)} = \mathbf{U}_{\text{time}}\mathbf{S^c}_{(2)}$ with $\mathbf{R^s}_{(2)} \in \mathbb{R}^{T\times CS}$. Unfolding along mode 2 corresponds to transposing each $\mathbf{R}^s_{::s}$ and concatenating all subjects, i.e., $\mathbf{R^s}_{(2)} = [(\mathbf{R^s}_{::1})^T|...(\mathbf{R^s}_{::S})^T]$, and equivalently for $\mathbf{S^c}_{(2)} = [(\mathbf{S^c}_{::1})^T|...(\mathbf{S^c}_{::S})^T]$. The first C columns of $\mathbf{R^s}_{(2)}$ and $\mathbf{S^c}_{(2)}$ thus contain the weighted connectivity averages and connectivity maps. Using simple linear algebra we can reduce equation $\mathbf{R^s}_{(2)} = \mathbf{U}_{\text{time}}\mathbf{S^c}_{(2)}$ to $(\mathbf{R^s}_{::1})^T = \mathbf{U}_{\text{time}}(\mathbf{S^c}_{::1})^T$, which is equivalent to

$$\mathbf{R^s}_{::1} = \mathbf{S^c}_{::1}\mathbf{U}^T_{\text{time}}. \tag{3}$$

Thus, average dynamic connectivity $\mathbf{R^s}_{::1}$ is decomposed into group connectivity maps $\mathbf{S^c}_{::1}$ and associated time courses $\mathbf{U}_{\text{time}}$.

We then determined which connectivity maps were related to the paradigm by using $\mathbf{U}_{\text{time}}$ as regressors in the following

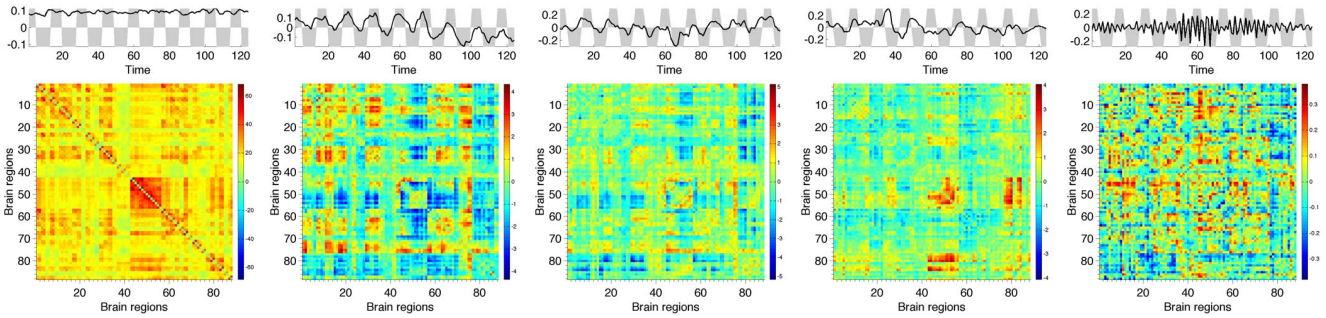

Figure 2: Some of the group connectivity maps $\mathbf{S^c}_{:i1}$ with $i = 1, 2, 3, 4, 100$, resulting from the HOSVD of the multi-subject dynamic networks and associated time courses (black) overlaid on the paradigm (gray shading). Group maps were reshaped and symmetrized. The subject loadings (i.e., first column of $\mathbf{U}_{\text{subjects}}$) were $[.25, .27, .22, .25, .37, .21, .26, .21, .29, .24, .25, .25, .29, .20, .26]$.

general linear model:

$$\mathbf{y} = \mathbf{U}_{\text{time}}\boldsymbol{\beta} + \boldsymbol{\epsilon}, \tag{4}$$

where $\mathbf{y} \in \mathbb{R}^T$ is a demeaned, moving average of the paradigm (0 = rest, 1 = movies) with $\Delta t = 40$; $\boldsymbol{\beta} \in \mathbb{R}^T$ the regression coefficients; and $\boldsymbol{\epsilon}$ the noise term. Note that the ordinary least-squares solution can be obtained as $\boldsymbol{\beta} = \mathbf{U}_{\text{time}}^T\mathbf{y}$.

C. Prediction of the paradigm in an unseen subject

We want to examine how well the linear combination of the group connectivity maps determined by (4) can predict the paradigm in an unseen subject. Therefore, we apply the HOSVD within a leave-one-subject-out cross-validation loop:

1) Estimate the group connectivity maps $\mathbf{S^c}_{::1}$ and associated time courses $\mathbf{U}_{\text{time}}$ of $S-1$ subjects.
2) Estimate the best linear combination to predict the paradigm: $\boldsymbol{\beta} = \mathbf{U}_{\text{time}}^T\mathbf{y}$.
3) Estimate the time courses of the group connectivity maps for the unseen subject: $\mathbf{A}_{\text{time}}^T = (\mathbf{S^c}_{::1})^{-1}\mathbf{R}$, where $\mathbf{A}_{\text{time}} \in \mathbb{R}^{T\times T}$ contains the time courses. We here interpreted $\mathbf{U}_{\text{time}}$ of Eq. (3) as coefficients in the "connectivity" space ($\mathbf{U}_{\text{time}}^T = (\mathbf{S^c}_{::1})^{-1}\mathbf{R^s}_{::1}$), and we obtain them for an unknown dynamic connectivity matrix $\mathbf{R}$ by projection.
4) Predict the experimental paradigm $\tilde{\mathbf{y}} = \mathbf{A}_{\text{time}}\boldsymbol{\beta}$ for the unseen subject using the weights $\boldsymbol{\beta}$ learned from the $S-1$ other subjects.

We evaluated the quality of the prediction by calculating the correlation between the predicted and real paradigm. Steps $1-4$ were repeated for all subjects and using $K = 1, 2, ..., T$ predictors. We ranked the importance of the different components by averaging the weights $\boldsymbol{\beta}$ across the S folds.

We compared the prediction against the model $\mathbf{y} = \mathbf{B}_{\text{time}}\boldsymbol{\beta} + \boldsymbol{\epsilon}$, where $\mathbf{B}_{\text{time}} \in \mathbb{R}^{T\times C}$ contained the average strength of each pair-wise correlation across the other $S-1$ subjects. We ranked the connections according to their weight.

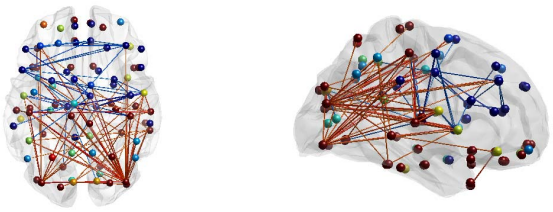

Figure 3: Visualization of the strongest connections in map 2 in brain space. Each sphere represents one brain region and its color is modulated by its degree.

III. Results

A. Group connectivity maps

In Fig. 2 we show some of the group connectivity maps in $\mathbf{S^c}_{::1}$ with associated time courses. The first map is all-positive and tracks global connection strength across time. It shows "conventional" connectivity clusters, such as among visual regions ($43-58$). The time course of the second map shows a striking resemblance with the paradigm, which is unknown to the tensor decomposition. We also visualize this component in Fig. 3, where connections in red contribute more strongly during rest and blue ones during movies. Red connections include a visual-parietal network, and visual-cingulate connections, while blue connections are mostly localized in frontal regions.

Higher components (e.g., $\mathbf{S^c}_{:i1}$ with $i = 100$ in Fig. 2) have rapidly oscillating time courses and likely represent noise. $\mathcal{S}$ has the same size as $\mathcal{R}$ in HOSVD (i.e. we obtain T components), but removing such components could help to reduce noise in dynamic networks (similar to truncated SVD) and here we use $\boldsymbol{\beta}$ to define components of interest.

B. Paradigm prediction

We then predicted the time course of the paradigm in a previously unseen subject using the maps and time courses learnt from all other subjects (steps 2-4). Fig. 4 shows the predicted time courses for 3 example subjects. For two of

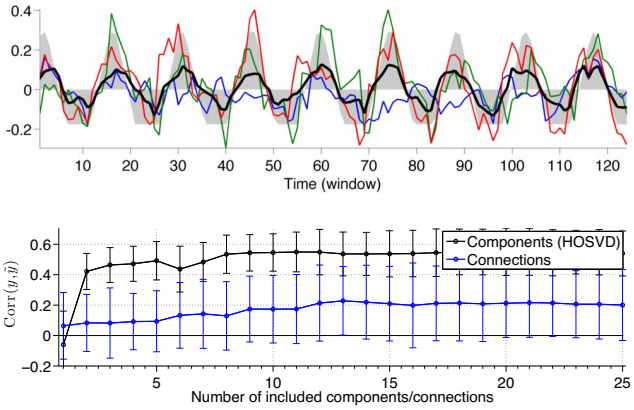

Figure 4: (top) Predicted time courses using 8 components for 3 example subjects (blue, green and red lines), and average predicted time course across all subjects (black line), overlaid on the experimental paradigm (gray). (bottom) Correlation between the predicted and real paradigm as a function of number of included components (black) or connections (blue), error bars show the standard deviation across folds.

them (green and red), the time course clearly tracks the paradigm, while the prediction failed for the third subject (blue). The folds-averaged correlation between the predicted time course and the paradigm flattened at $\rho = 0.53 \pm 0.13$ for 8 components (Fig. 4). Including the second component resulted in an average correlation of $\rho = 0.42 \pm 0.12$, and it had the largest weight across all folds. The next largest weights were for components 3 and 8. Predictions using connections with the K largest weight performed less well, flattening at an average correlation of $\rho = 0.21 \pm 0.22$, and no improvement when including up to 100 connections ($\rho = 0.18 \pm 0.20$, $\boldsymbol{\beta}$ contained 124 non-zero weights).

IV. Conclusion

We proposed a novel approach based on tensor decomposition to extract whole-brain connectivity patterns from multi-subject dynamic networks. The extracted maps can be related to the experimental paradigm by regression of the associated time courses. Using cross-validation, we identified a network of connections that differed between movies and rest, and that generalizes to the out-of-fold subject. We found that most connections were stronger during rest, especially of visual regions, and those of the thalamus during movies, which is in accordance with previous findings [2], where the authors discriminated between the two states using "static" connectivity graphs. The HOSVD allowed to obtain connectivity maps, subject loadings, and associated time courses with strong resemblance to the experimental paradigm without any prior knowledge of the two states.

We believe that the proposed approach holds promise to reveal subtle patterns in dynamic brain connectivity for a wide variety of cognitive states. The currently proposed regression is only a first step to learn network correlates of these states and its success highly benefits from the effective dimensionality reduction by the HOSVD. However, future work should look into more sophisticated tools from machine learning and apply the scheme for online decoding of brain states.

Acknowledgment

The authors thank Dr. H. Eryilmaz, Prof. P. Vuilleumier and Prof. S. Schwartz for providing the fMRI data. This work was supported by the Swiss National Science Foundation (grant PP00P2-123438), the Société Académique de Genève, the FOREMANE foundation, and the Center for Biomedical Imaging (CIBM).

References

[1] D. Bassett, N. Wymbs, M. Porter, P. Mucha, J. Carlson, and S. Grafton, "Dynamic reconfiguration of human brain networks during learning," *Proc. Natl. Acad. Sci. USA*, vol. 108, no. 18, pp. 7641–7646, May 2011.

[2] J. Richiardi, H. Eryilmaz, S. Schwartz, P. Vuilleumier, and D. Van De Ville, "Decoding brain states from fMRI connectivity graphs," *NeuroImage*, vol. 56, no. 2, pp. 616–626, May 2011.

[3] I. Cribben, R. Haraldsdottir, L. Y. Atlas, T. D. Wager, and M. A. Lindquist, "Dynamic connectivity regression: determining state-related changes in brain connectivity.," *Neuroimage*, vol. 61, no. 4, pp. 907–920, Jul 2012.

[4] C. Chang and G. Glover, "Time-frequency dynamics of resting-state brain connectivity measured with fMRI," *NeuroImage*, vol. 50, no. 1, pp. 81–98, Mar. 2010.

[5] E. A. Allen, E. Damaraju, S. M. Plis, E. B. Erhardt, T. Eichele, and V. D. Calhoun, "Tracking whole-brain connectivity dynamics in the resting state," *Cereb Cortex*, p. in press, 2012.

[6] A. Krishnan, L. J. Williams, A. R. McIntosh, and H. Abdi, "Partial least squares (PLS) methods for neuroimaging: a tutorial and review.," *NeuroImage*, vol. 56, no. 2, pp. 455–475, May 2011.

[7] C. F. Beckmann and S. M. Smith, "Tensorial extensions of independent component analysis for multisubject fmri analysis.," *NeuroImage*, vol. 25, no. 1, pp. 294–311, Mar 2005.

[8] G. Varoquaux, S. Sadaghiani, P. Pinel, A. Kleinschmidt, J. B. Poline, and B. Thirion, "A group model for stable multi-subject ica on fmri datasets.," *Neuroimage*, vol. 51, no. 1, pp. 288–299, May 2010.

[9] T. G. Kolda and B. W. Bader, "Tensor decompositions and applications," *SIAM Rev.*, vol. 51, no. 3, pp. 455–500, Aug. 2009.

[10] N. Leonardi and D. Van De Ville, "Tight wavelet frames on multislice graphs," *Signal Processing, IEEE Transactions on*, p. in press, 2013.

[11] L. De Lathauwer, B. De Moor, and J. Vandewalle, "A multilinear singular value decomposition," *SIAM J. Matrix Anal. Appl*, vol. 21, pp. 1253–1278, Apr. 2000.

[12] H. Eryilmaz, D. V. D. Ville, S. Schwartz, and P. Vuilleumier, "Impact of transient emotions on functional connectivity during subsequent resting state: A wavelet correlation approach.," *Neuroimage*, vol. 54, no. 3, pp. 2481–2491, Oct 2011.

[13] N. Tzourio-Mazoyer, B. Landeau, D. Papathanassiou, F. Crivello, O. Etard, N. Delcroix, B. Mazoyer, and M. Joliot, "Automated anatomical labeling of activations in SPM using a macroscopic anatomical parcellation of the MNI MRI single-subject brain," *NeuroImage*, vol. 15, no. 1, pp. 273–289, Jan. 2002.

[14] R. Harshman and S. Hong, "'Stretch' vs 'slice' methods for representing three-way structure via matrix notation," *J. Chemometrics*, vol. 16, no. 4, pp. 198–205, Apr. 2002.